CrossMark

ORIGINAL ARTICLE

A high resolution measurement of the morning ABL transition using distributed temperature sensing and an unmanned aircraft system

C. W. Higgins[1] · M. G. Wing[2] · J. Kelley[1] · C. Sayde[1,3] ·
J. Burnett[2] · H. A. Holmes[4]

Abstract We used an unmanned aircraft system (UAS) to lift and suspend distributed temperature sensing (DTS) technologies to observe the onset of an early morning transition from stable to unstably stratified atmospheric conditions. DTS employs a fiber optic cable interrogated by laser light, and uses the temperature dependent Raman scattering phenomenon and the speed of light to obtain a discrete spatial measurement of the temperature along the cable. The UAS/DTS combination yielded observations of temperature in the lower atmosphere with high resolution (1 s and 0.1 m) and extent (85 m) that revealed the detailed processes that occurred over a single morning transition. The experimental site was selected on the basis of previous experiments and long term data records; which indicate that diurnal boundary layer development and wind sectors are predictable and consistent. The data showed a complex interplay of motions that occur during the morning transition that resulted in propagation and growth of unstable wave modes. We observed a rapid cooling of the air aloft (layer above the strong vertical temperature gradient) layer directly after sunrise due to vertical mixing followed by an erosion of the strong gradient at the stable layer top. Midway through the transition, unstable wave modes were observed that are consistent with Kelvin–Helmholtz motions. These motions became amplified through the later stages of the transition.

✉ M. G. Wing
michael.wing@oregonstate.edu

1   Biological and Ecological Engineering, Oregon State University, Corvallis, OR, USA

2   Forest Engineering, Resources, and Management, Oregon State University, Corvallis, OR, USA

3   Biological and Agricultural Engineering, North Carolina State University, Raleigh, NC, USA

4   Atmospheric Sciences Program, Department of Physics, University of Nevada, Reno, Reno, NV, USA

1 Introduction

The morning transition of the atmospheric boundary layer (ABL), from a stable stratification to an unstable stratification, is associated with rapid growth of the planetary boundary layer and turbulence generation. Sunrise begins a cascade of physical events that occur within a short timeframe over the entire lower boundary layer profile. There are two potential sources of energy that can drive this process: (1) the buoyant force that results from the radiative heating of the ground after sunrise, and (2) the kinetic energy contained in the atmospheric flow aloft. Open questions remain as to the exact nature of this transition, the relative importance of each source of energy and the sequence of small scale processes that interact during the transition.

Several studies have attempted to describe the morning transition with a set of timescales both experimentally (e.g., [2, 5, 20, 24]) and numerically using large-eddy simulations (e.g., [4, 9, 10, 33]). Numerical studies allow for systematic investigations of boundary conditions on the flow. However it can be difficult to capture the full range of scales during transitions with numerical models, as length scales range from centimeters in the stable boundary layer (SBL) to kilometers in the fully developed convective boundary layer (CBL). Field studies can provide insights into flow behaviors across these scales, complementing and improving models of complex flow behavior. This is especially true for flow over heterogenous surface conditions and complex topography, where flow patterns and pressure effects are influenced by orography and variability in surface heating [18]. Beare [4] addresses this issue and modeled all scales through the morning transition by simulating the full boundary layer transition from a stable boundary later (SBL) to convective boundary layer (CBL). He found that shear dominated during the early stages of SBL transition and buoyancy dominated during the later stages of transition during CBL growth.

The results of Beare [4] are consistent with results from the two experimental studies of Angevine et al. [2] and Lapworth [24], who demonstrated that while surface warming enables the transition from stable to unstable stratification, entrainment of warm air aloft due to shear driven turbulence is primarily responsible for eroding the SBL during the morning transition. Both of these studies investigated the timing of the morning transition and the onset of the CBL growth using a combination of tower (sonic anemometer, temperature) and vertical profiler data (temperature, wind speed).

Limited spatial resolution in the available data make it difficult to investigate the entrainment processes that lead to the erosion of the SBL [9]. Typically, experiments to quantify the physical mechanisms contributing to turbulence in the atmospheric surface layer rely on tower measurements, tethered balloon data, or temperature profilers such as SODAR, LIDAR, and radio acoustic sounding systems. Long-term records of tower data are typically limited to less than ten measurement heights, with the lowest wind speed sensor at 10 m and temperature sensor at approximately 2 m (e.g., [1, 24]). Vertical profilers provide more detailed data regarding the vertical structure of the atmosphere, however the vertical sampling resolution is 15–60 m [13]. Unmanned aircraft system (UAS) provide an opportunity to increase the observable resolution, as demonstrated in Wildmann et al. [38], Martin et al. [25] and Bonin et al. [7]. We hypothesize that critical localized intermittent processes (CLIPS) are unresolved with currently available technologies, and a more highly resolved approach is needed.

A detailed observation of the transition O(sub-meter) vertical resolution, O(1s) temporal resolution of the transition process has yet to appear in the literature (to our knowledge). If we are to evaluate the detailed events of the morning transition, concurrent high spatial and

temporal resolution is required. Thus, we need to move beyond discrete measurements to a distributed approach. This paper presents high resolution measurements of the vertical temperature profile in the boundary layer because it is an indicator of mixing and stabilizing processes that drive transport of trace gasses, water vapor, and air pollutants in the lower troposphere [34].

Distributed Temperature Sensing (DTS) technology can measure temperature along a fiber optic cable that can extend several km in length with very high spatial and temporal resolutions (e.g. [30, 35, 41]). The measurement principle relays on quantifying the Raman optical change in scattering of a laser pulse sent into a fibe optic cable [11, 22, 31, 32, 36, 39]. As the laser pulse travel along the cable, part of its energy will either be reflected back at the same wavelength of the original signal or scattered at longer or shorter wavelength. The frequency-shifted scattering is called Raman-scattering. The photons scattered at longer wavelength are called Stokes and the photons scattered at shorter wavelength are called anti-Stokes. The anti-Stokes relative intensity is linearly related to the temperature of the scattering location, while the Stokes relative intensity is independent of the temperature. DTS instruments are equipped with photon detectors that can time the return and measure the intensity of Stokes and anti-Stokes that scatter back. The location of the measurement is determined by the travel time of the photons. Temperature along the cable is calculated from the measured ratio of Stokes/anti-Stokes. For detailed overview of the calibration procedures, see Hausner et al. [15] and van de Giesen et al. [37].

A proliferation of DTS measurements for environmental applications began with Selker et al. [31]. The development of DTS technology has revealed a new path to measure temperature at high temporal and spatial resolutions [36]. So far, DTS measurements have been used and proven successful in many hydrological systems [31, 32]. The DTS method also shows great potential in atmospheric boundary layer measurement. There are currently a limited number of pioneering experiments that used fiber optic DTS in atmospheric measurement. Thomas et al. [35] and Zeeman et al. [41] arranged the fiber optic cable into multi-dimensional arrays to measure small scale processes in the surface layer. Krause et al. [21] installed a fiber optic system under the forest canopy to monitor the thermal patterns of the vegetation cover. Keller et al. [19] suspended a fiber optic cable below a small blimp to measure temperature profiles of the near surface atmospheric boundary layer. Petrides et al. [26] used a fiber optic installation to capture the temperature change near a stream due to shading effects. Tyler et al. [36] discuss the quality of the DTS data. Sayde et al. [30] extended the capabilities of DTS to measure wind speed. With the exception of Keller et al. [19], all of these experiments placed fiber optic cable(s) near the ground (from 1 to 8 m). In Keller et al. [19] the fiber optic cable was lifted to a height of 100 m, but the authors noted that the tethered balloon tends to move by the corresponding wind drag under strong wind conditions. This deficiency of the balloon can be overcome by employing small, remotely controlled UAS. UAS possesse other advantages such as a precisely controlled flying path, the ability to fly over complex landscapes, and the capacity to immediately replicate the measurement at the same location [40].

UAS have already been used in atmospheric boundary layer research as movable platforms to support suites of point measurements (e.g. temperature) [6, 23, 29] where the UAS were controlled to fly vertical or horizontal transects at a higher elevation (200–1500 m). Martin et al. [25] used a fixed wing UAS platform to measure fine scale variability at the entrainment zone at the boundary layer top. Bonin et al. [7] used the helical geometry of UAS ascent and decent to measure the temperature structure function

in a morning transition. Wildmann et al. [38] discovered increased horizontal wind variance as altitude increases with UAS profiles performed throughout a morning transition. Platis et al. [27] measured an order of magnitude increase in the temperature structure parameter inside the entrainment zone during the morning transition with a UAS. Hemingway et al. [16] measured vertical profiles of temperature and humidity at 1.5-3 m resolution. Greatwood et al. [14] used rotorwing UAS to rapidly ascend (5 m/s) through the boundary layer and measure the temperature, humidity and methane concentration. The UAS-transect approach can yield detailed vertical information and has given insight into the large-scale structure of the lower atmosphere. In this study, we enhance the UAS transect approach with an alternative measurement technology, fiber optic DTS. DTS and UAS together have the potential to resolve even fine scale (spatial and temporal) atmospheric processes through non-stationary transitions in the atmospheric boundary layer.

This paper will describe a measurement campaign and demonstrate the suitability of fiber optic DTS combined with a UAS in atmospheric boundary layer measurement. The experiment was carried out in August 2014 in an irrigated agricultural field (near Hermiston, Oregon at 45.7°N 119.4°W, at 280 m elevation). An array of wind turbines is located adjacent to these fields. The site was selected with the aim to measure the atmospheric boundary layer dynamics during the morning transition.

2 Experimental setup

Figure 1 shows a schematic drawing of the experimental setup. The DTS instrument was an ULTIMA^{TM} unit (Silixa, Elstree, UK) with a sampling resolution of 12.5 cm, a measurement time resolution of 1 s, and a temperature resolution of 0.1 °C. The fiber optic
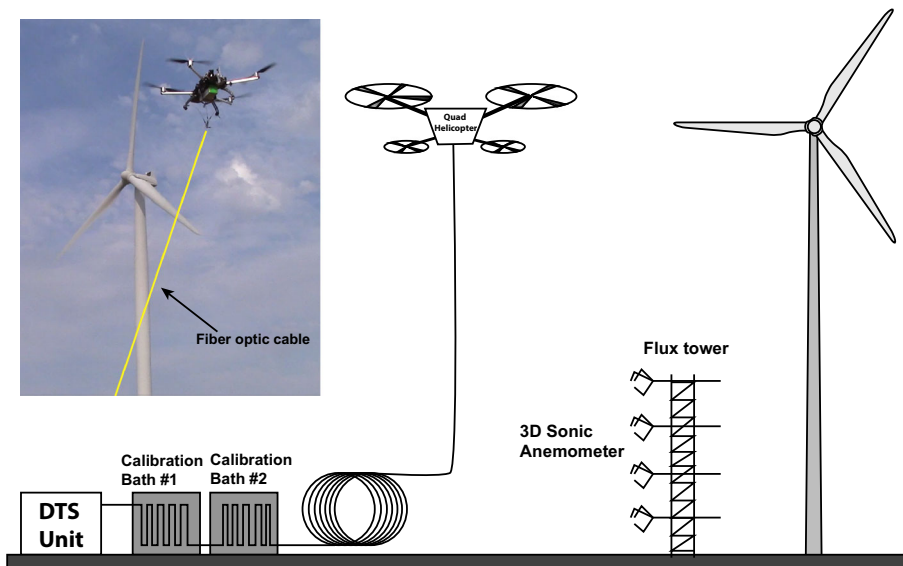

Fig. 1 Schematic of the experimental setup. The fiber optic cable in the photo was color enhanced to increase contrast with the background sky

cable used in this experiment is a single 50 μm glass fiber, jacketed with Kevlar and white plastic. The outer diameter of the cable was 900 μm. The total length of the cable was approximately 200 m (max allowable length for this instrument was 2000 m). Approximately 120 m of cable was flown with the balance used for calibration baths, and connecting the instrument placement to the flight location. For a flying period of 25 min, the error induced by solar heating on the cable can be considered negligible [12]. The cable was connected to the DTS unit and passed through two calibration baths (one with ice-water mix and one with water) which served as temperature references. The temperatures inside the water baths were monitored with the PT 100 thermometers connected to the ULTIMA^{TM} unit.

We used the Matrix quadcopter as our UAS platform (Turbo Ace 2015). The Matrix is constructed of aluminum and carbon fiber materials and is battery powered. Maximum flight time for the Matrix with a 16,000 mAh battery is approximately 30 min with a 0.5 kg payload. The Matrix has four carbon fiber propellers and each propeller is 38 cm in diameter. When all four propellers are installed the diameter of the Matrix approaches 1 m. We obtained a Certificate of Authorization (COA) from the Federal Aviation Administration (FAA) to support our UAS operations with the Matrix. The total flight time of observation was limited to 2 flights for a total of ∼ 1 h of observation. We recognize that this observation period limits the scope of inference of the study, and thus focus on the onset of the morning transition.

We attached the fiber optic cable to a tether system that was connected to the bottom of the Matrix quadcopter. The Matrix climbed to a height of approximately 120 m, lifting the suspended fiber optic cable, and hovered until battery voltage levels dropped to levels that could not support additional sustained flight time. The flight times varied between 20 and 30 min, and were affected by temperature and battery health. During the ascent and descent phases of the flight, tension in the cable was controlled to avoid breakage and cable kinking. It was found that coiling the fiber optic cable loosely, three workers were able to manually eliminate cable twist and allow the quadcopter to pull cable from the coil without excess tension. The DTS cable was operated in a single-ended configuration in this experiment.

A 10 m tower was also instrumented at the flight location to capture the surface layer velocity profiles and turbulence parameters. Four IRGASON 3D sonic anemometers (Campbell Scientific Inc., Utah) were installed at the elevations of 1.1, 2.7, 4.8, and 7.7 m respectively. These instruments sampled the three dimensional wind vector, the sonic temperature, mixing ratio and CO_2 concentration at 10 Hz. The tower provides typical micro-meteorological measurements of the morning transition, including bulk and flux Richardson number, friction velocity, and the Obukhov length, which are used to give context to the DTS measurements.

Seven flights occurred over a two-day interval. Five flights were performed in the evening of August 27, 2014 and two flights were performed in the morning of August 28, 2014 to capture a detailed observation of the morning transition upwind of the active wind turbines. Note that the total observation time of the morning transition will not capture the later stages of the morning transition, thus we focus on the initiation of the transition. Platis et al. [27] presented eight profiles through a morning transition, and while the complete transition throughout the entire boundary layer depth took place over the course of several hours, the near surface stability had changed fully in approximately 1.5 h (a total of 3 profiles presented in Platis). In this study we present nearly 2952 profiles throughout the first ∼ 1 h of the transition. The range of those profiles are from surface level to ∼ 85 m above surface level (height was limited by FAA COA).

The DTS measurements were calibrated with the method provided in Hausner et al. [15]. For plotting purposes, the data were low pass filtered with a 'top hat filter' that had a characteristic time scale of 20 s and a characteristic length scale of 1 m. Only the first 85 m of the 120 m profile are retained for analysis to eliminate possible rotor downwash effects. We calculated the distance below the UAS such that the downwash would be advected away from the fiber optic cable by a minimum mean wind speed under a worst case scenario: no turbulent degradation of the downwash, and the speed of motion equal to the jet centerline velocity. From Pope [28], the downwash velocity at centerline $\sim 1/x$, and width of downwash $\sim 0.1x$. The time of travel of a fluid parcel to a point below the UAS is calculated from the integral of the downward centerline velocity. If the horizontal velocity is greater than the downwash width divided by the travel time, then the downwash will not impact the measurements as it will have been advected downstream and out of the interrogation area. We chose 0.15 m/s or greater ambient wind speeds in our calculation which resulted in 35 m below the rotors.

3 Results and discussion

Filtered data of the potential temperature are presented in Fig. 2. Sunrise initiated a rapid vertical mixing above the stable boundary layer as displayed in filtered data (Fig. 2) that resulted in an immediate *cooling* of the air aloft directly following sunrise. Then, a slow asymmetric degradation of the stable temperature gradient at the stable boundary layer top (~ 5 m) occurs over a 30 min period. The degradation is more severe above the stable layer. Finally, an unstable mode visible at $\sim 6{:}50$ begins to grow. This unstable mode continues to grow and initiates further entrainment.

The presence of an unstable mode that is amplified at the time of transition suggests a classical Kelvin–Helmholtz linear stability approach may yield fruitful insights. Further, it suggests that the kinetic energy of the upper flow (and the associated shear at the top of the shallow stable layer) is critical for the transition in addition to the ground heating, and that the transition may be capable of beginning before the heat flux becomes positive at the land surface. If the onset of the morning transition arises from this instability then the Kelvin–Helmholtz linear stability analysis should predict the wavelength of unstable mode.
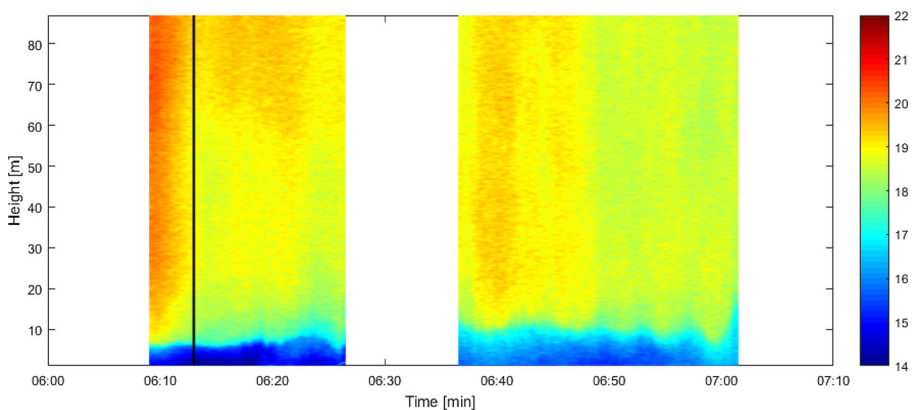

Fig. 2 Two flights through the morning transition on the morning of August 28th, 2014. Local sunrise is at 6:13 AM. Color indicates temperature measured in Celsius

Following Chandrasaker [8], the instability of two fluids of differing density and velocity can be analyzed with linear perturbation theory to show that all modes with wavenumbers

$$k > \frac{g(\alpha_1 - \alpha_2)}{\alpha_1 \alpha_2 (\Delta U)^2 \cos^2 \varphi} \tag{1}$$

will be unstable. In Eq. 1, g is the acceleration due to gravity, ΔU is the difference in velocity between the upper and lower fluids (measured with the acoustic anemometers), φ is the angle between k and U, and the parameters $\alpha_1 = \rho_1/(\rho_1 + \rho_2)$ and $\alpha_2 = \rho_2/(\rho_1 + \rho_2)$ are non-dimensional ratios of air density. The subscript 1 refers to the lower fluid, and subscript 2 refers to the upper. In this case $\rho_2 < \rho_1$. The angle φ is set to zero to find the minimum unstable wave mode. Then, the ideal gas law, with assumed constant pressure, is used to link temperatures and density, resulting in:

$$k_{\min} = \frac{g}{(\Delta U)^2} \left(\frac{T_2}{T_1} - \frac{T_1}{T_2} \right), \tag{2}$$

where T_1 and T_2 are the air temperatures in each layer expressed in Kelvin with the condition that $T_2 > T_1$. Recall that this stability analysis assumes that there is no other input of energy to the system (e.g. a surface heating) and is solely the balance between the available kinetic energy of the flow and the existing stabilizing buoyant stratification. Taking values at approximately 6:45 from Fig. 2: T2 = 19 °C at 10 m, T1 = 17 °C at 15 m. The tower observed a $\Delta U = 2$ m/s between the upper and lower instruments. With these values, Eq. 2 yields a predicted wavenumber of 0.034 m^{-1}. Concurrently, the period of the observed oscillation feature (4 min) can be observed directly in Fig. 2 (after 6:50). Taylor's hypothesis is employed [17] using the measured vertically averaged wind speed of ~ 1 m/s (we assume that the wave structures are advected at the mean wind at the transition zone). The observed unstable wavenumber, taken directly from Fig. 2, is 0.026 m^{-1}. This value is quite close, yet still below the theoretical minimum given the observed temperatures and velocities (0.033 m^{-1}) for a simple 2 layer case with no surface heating. The theoretical minimum would decrease if (1) the temperature difference is reduced across the top of the stable boundary layer, or (2) there is an additional source of energy that assists in performing the work to overturn the stratification. In case 1, since the actual density stratification across the measured transition is not sharp, as assumed in the perturbation analysis, the thermal stratification is weaker than modeled, and could be a reason for the lower than expected unstable wavenumber. Further, in case 2, solar energy can provide a secondary source of energy through ground heating which contributes to the transition. Our conclusion is that (1) shear is a principle source of energy for the onset of the morning transition in this case, and (2) this energy is supplemented by the solar heating at the onset of the morning transition. These observations are consistent with Angevine [3] who stated that the warming of the boundary layer was driven primarily due to entrainment.

Our observations indicate that the morning transition, for this observation, occurs in the following steps:

1. Local sunrise.
2. Vertical mixing above the stable surface layer extending into the air aloft (above ~ 5 m), timescale $O(1)$ minute.

3. Erosion of the temperature gradient at the top of the stable surface layer caused by vertical mixing from above, and solar heating below. Timescale varies, in our case this was ~ 25 min.
4. Onset of unstable oscillatory wave motions reminiscent of a Kelvin–Helmholtz instability, in which timescale is dependent on the wind speed and stratification but can be bounded. Wavenumber of oscillation is less than the theoretical minimum given in Eq. 2, O(minutes).
5. Rapid vertical entrainment and unstable boundary layer growth. Timescale not fully characterized by the current observations.

The timing of these events is not coincident with known stability indicators (Fig. 3), and is likely driven by the structure and turbulence properties of the air aloft. The Obukhov length, $L = \frac{-u_*^3 \bar{T}_v}{kg\overline{w'T_v'}}$ and the Richardson number (Ri), $Ri = \frac{(g/\bar{T}_v)\overline{w'T_v'}}{u'w'\left(\frac{\partial U}{\partial z}\right)+v'w'\left(\frac{\partial V}{\partial z}\right)}$ as observed from tower data during the transition, did not coincide with the onset of oscillatory motions. The Richardson number indicated that the transition occurred at the start of step 3 above (critical Richardson number of 0.25). This is logical from a stability perspective, as a simple system of continuously varying density and velocity can be stable well after Ri is less than 0.4 [8, p. 494]. That is, for the case under consideration, a Ri < 0.25 is sufficient for a transition, but does not mean a transition must occur. The stability parameter based on the Obukhov length indicated that the transition occurred in step 5, which is logical as it is strongly tied to the behavior of the heat flux, and changes in the heat flux are most observable in step 5.

To investigate the physical mechanisms leading to the destruction of the nocturnal boundary layer experiments must collect data that resolves and localizes the stable boundary layer top. Gradients at the boundary layer top are sharp (e.g., large changes in less than 1 m as seen in Fig. 2). The position of the boundary layer top is not known a priori, and it moves throughout the transition. Measurements must have sufficient spatial
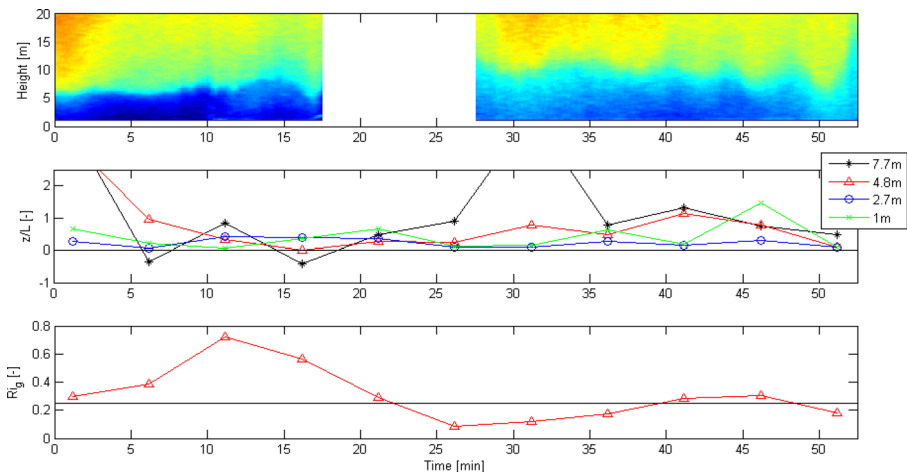

Fig. 3 Morning transition of August 28th, 2014 and the corresponding flux tower measurement. Top panel shows the temperature gradient for the first 20 m above ground surface. Middle panel shows the stability parameter values at four elevation where the 3D sonic anemometers were installed. The bottom panel shows the Richardson number

resolution and sufficient temporal density to capture the mixing phenomena, and also be distributed throughout the boundary.

4 Conclusions

The results presented in this paper demonstrate that UAS combined with DTS method is a promising system that can be used in atmospheric boundary layer measurements to provide temporally high resolution data at heights equal to tall permanent towers. Such a system can integrate the advantages from both technologies and has great potential in the future atmospheric measurement efforts. Angevine et al. [2] suggest that the shear mixing is a strong driver of the morning transition; the wind profile that manifests during the transition time modulates the timescales, and that the wind shear is a source of much of the observed scatter in their plots. If the mixing is shear driven, then it is reasonable to suppose that there is a competition between a stable buoyant forcing and the destabilizing effects of shear instability. Our results corroborate this observation and suggest that the classical stability parameters (Richardson number and Obukhov length) bracket the transition, but do not describe the transition adequately. Since the timescale of this unstable mode is directly related to the velocity and temperature gradients, it is conceivable that a relationship exists between the transition timescale and the wavelength of the unstable mode, but further study under a variety of atmospheric conditions is needed.

Although the UAS-DTS system opens possibilities for temperature measurements in the upper atmospheric boundary layer, there are safety considerations. All local and federal laws should be obeyed at the time of flight. Flying UAS in United States territorial sky requires permission from FAA. Secondly, two experienced pilots are needed to operate the UAS as regulated. Finally, the flying period is limited by the battery capacity of the UAS which may be the limiting factor for longer measurements. There are consistent improvements in battery capacity however, so this consideration may be reduced in future years.

References

1. Angevine WM, Grimsdell AW, Hartten LM, Delany AC (1998) The Flatland boundary layer experiments. Bull Am Meteor Soc 79(3):419–431
2. Angevine WM, Baltink HK, Bosveld FC (2001) Observations of the morning transition of the convective boundary layer. Bound Layer Meteorol 101(2):209–227
3. Angevine WM (1999) Entrainment results including advection and case studies from the Flatland boundary layer experiments. J Geophys Res Atmos 104(D24):30947–30963
4. Beare RJ (2008) The role of shear in the morning transition boundary layer. Bound Layer Meteorol 129(3):395–410
5. Bennett LJ, Weckwerth TM, Blyth AM, Geerts B, Miao Q, Richardson YP (2010) Observations of the evolution of the nocturnal and convective boundary layers and the structure of open-celled convection on 14 June 2002. Mon Weather Rev 138(7):2589–2607

6. Bonin T, Chilson P, Zielke B, Fedorovich E (2013) Observations of the early evening boundary-layer transition using a small unmanned aerial system. Bound Layer Meteorol 146:119–132
7. Bonin TA, Goines DC, Scott AK, Wainwright CE, Gibbs JA, Chilson PB (2015) Measurements of the temperature structure-function parameters with a small unmanned aerial system compared with a sodar. Bound Layer Meteorol 155(3):417–434
8. Chandrasaker S (1961) Hydrodynamic and hydromagnetic stability. Dover ed. Dover Publucation, NY, pp 494
9. Conzemius RJ, Fedorovich E (2006) Dynamics of sheared convective boundary layer entrainment. Part I: methodological background and large-eddy simulations. J Atmos Sci 63(4):1151–1178
10. Conzemius RJ, Fedorovich E (2006) Dynamics of sheared convective boundary layer entrainment. Part II: evaluation of bulk model predictions of entrainment flux. J Atmos Sci 63(4):1179–1199
11. Dakin JP, Pratt DJ, Bibby GW, Ross J (1985) Distributed optical fiber Raman temperature sensor using a semiconductor light-source and detector. Electron Lett 21(13):569–570. https://doi.org/10.1049/el:19850402
12. De Jong SAP, Slingerland JD, van de Giesen NC (2015) Fiber optic distributed temperature sensing for the determination of air temperature. Atmos Meas Tech 8(1):335–339
13. Emeis S, Schäfer K, Münkel C (2008) Surface-based remote sensing of the mixing-layer height—a review. Meteorol Z 17(5):621–630
14. Greatwood C, Richardson TS, Freer J, Thomas RM, MacKenzie AR, Brownlow R, Lowry D, Fisher RE, Nisbet EG (2017) Atmospheric sampling on ascension island using multirotor UAVs. Sensors 17(6):1189
15. Hausner MB, Suárez F, Glander KE, Selker JS, Tyler SW (2011) Calibrating single-ended fiber-optic Raman spectra distributed temperature sensing data. Sensors 11(11):10859–10879. https://doi.org/10.3390/s111110859
16. Hemingway BL, Frazier AE, Elbing BR, Jacob JD (2017) Vertical sampling scales for atmospheric boundary layer measurements from small unmanned aircraft systems (sUAS). Atmosphere 8(9):176
17. Higgins CW, Froidevaux M, Simeonov V, Vercauteren N, Barry C, Parlange MB (2012) The effect of scale on the applicability of Taylor's frozen turbulence hypothesis in the atmospheric boundary layer. Bound Layer Meteorol 143(2):379–391
18. Kaimal JC, Finnigan JJ (1994) Atmospheric Boundary Layer Flows: Their Structure and Measurement. Oxford University Press
19. Keller CA, Huwald H, Vollmer MK, Wenger A, Hill M, Parlange MB, Reimann S (2011) Fiber optic distributed temperature sensing for the determination of the nocturnal atmospheric boundary layer height. Atmos Meas. Tech 4:143–149
20. Ketzler G (2014) The diurnal temperature cycle and its relation to boundary-layer structure during the morning transition. Bound Layer Meteorol 151(2):335–351
21. Krause S, Taylor SL, Weatherill J, Haffenden A, Levy A, Cassidy NJ, Thomas PA (2013) Fibre-optic distributed temperature sensing for characterizing the impacts of vegetation coverage on thermal patterns in woodlands. Ecohydrology 6:754–764
22. Kurashima T, Horiguchi T, Tateda M (1990) Distributed-temperature sensing using stimulated Brillouin-scattering in optical silica fibers. Opt Lett 15(18):1038–1040
23. Lampert A, Pätzold F, Jiménez MA, Lobitz L, Martin S, Lohmann G, Canut G, Legain D, Bange J, Martínez-Villagrasa D, Cuxart J (2016) A study of local turbulence and anisotropy during the afternoon and evening transition with an unmanned aerial system and mesoscale simulation. Atmos Chem Phys 16(12):8009–8021
24. Lapworth A (2006) The morning transition of the nocturnal boundary layer. Bound Layer Meteorol 119(3):501–526
25. Martin S, Beyrich F, Bange J (2014) Observing entrainment processes using a small unmanned aerial vehicle: a feasibility study. Bound Layer Meteorol 150:449–467
26. Petrides AC, Huff J, Arik A, van de Giesen N, Kennedy AM, Thomas CK, Selker JS (2011) Shade estimation over streams using distributed temperature sensing. Water Resour Res 47(7):W07601. https://doi.org/10.1029/2010WR009482
27. Platis A, Altstädter B, Wehner B, Wildmann N, Lampert A, Hermann M, Birmilli W, Bange J (2015) An observational case study of the influence of atmospheric boundary-layer dynamics on new particle formation. Bound Layer Meteorol. https://doi.org/10.1007/s10546-015-0084-y
28. Pope SB (2001) Turbulent flows. IOP Publishing, Bristol
29. Reuder J, Jonasse M, Olafsson H (2012) The Small Unmanned Meteorological Observer SUMO: recent developments and applications of a micro-UAS for atmospheric boundary layer research. Acta Geophys 60:1454–1473

30. Sayde C, Thomas CK, Wagner J, Selker J (2015) High-resolution wind speed measurements using actively heated fiber optics. Geophys Res Lett 42(22):10064–10073
31. Selker JS, Thévanaz L, Huwald H, Mallet A, Luxemburg W, van de Giesen N, Stejskal M, Zeman J, Westhoff MC, Parlange MB (2006) Distributed fiber-optic temperature sensing for hydrologic systems. Water Resour Res 42:W12202. https://doi.org/10.1029/2006WR005326
32. Selker JS, van de Giesen NC, Westhoff M, Luxemburg W, Parlange M (2006) Fiber-optics opens window on stream dynamics. Geophys Res Lett 33:L24401. https://doi.org/10.1029/2006GL027979
33. Sorbjan Z (2007) A numerical study of daily transitions in the convective boundary layer. Bound Layer Meteorol 123(3):365–383
34. Stull RB (1988) An introduction to boundary layer meteorology. Kluwer Academic Publishers, Dordrecht
35. Thomas C, Kennedy A, Selker J, Moretti A, Schroth M, Smoot A, Tufillaro N, Zeeman M (2012) High-resolution fibre-optic temperature sensing: a new tool to study the two-dimensional structure of atmospheric surface-layer flow. Bound Layer Meteorol 142(2):177–192. https://doi.org/10.1007/s10546-011-9672-7
36. Tyler SW, Selker JS, Hausner MB, Hatch CE, Torgersen T, Thodal CE, Schladow SG (2009) Environmental temperature sensing using Raman spectra DTS fiber-optic methods. Water Resour Res 45:W00D23. https://doi.org/10.1029/2008wr007052
37. Van de Giesen N, Steele-Dunne SC, Jansen J, Hoes O, Hausner MB, Tyler S, Selker J (2012) Double-ended calibration of fiber-optic Raman spectra distributed temperature sensing data. Sensors 12(5):5471–5485
38. Wildmann N, Rau GA, Bange J (2015) Observations of the early morning boundary-layer transition with small remotely-piloted aircraft. Bound Layer Meteorol 157(3):345–373
39. Williams GR, Brown G, Hawthorne W, Hartog AH, Waite PC (2000) Distributed temperature sensing (DTS) to characterize the performance of producing oil wells. In: Proceedings of SPIE, vol 4202, pp 39–54
40. Wing MG, Burnett J, Sessions J, Brungardt J, Cordell V, Dobler D, Wilson D (2013) Eyes in the sky: remote sensing technology development using small unmanned aircraft systems. J For 111(5):341–347
41. Zeeman MJ, Selker JS, Thomas CK (2015) Near-surface motion in the nocturnal stable boundary layer observed with fibre-optic distributed temperature sensing. Bound Layer Meteorol 154:189–205